Proceedings of the ASME 2018 International Design Engineering Technical Conferences and Computers and Information in Engineering Conference IDETC/CIE 2018
August 26-29, 2018, Quebec City, Quebec, Canada

DETC2018-85961

CALCULATION OF THE COLLISION-FREE PRINTING WORKSPACE FOR FULLY-CONSTRAINED CABLE-DRIVEN PARALLEL ROBOTS

Marc Fabritius
Christoph Martin *
Fraunhofer Institute for Manufacturing Engineering and Automation (IPA)
Robot and assistive systems
Stuttgart, 70569
Germany
marc.fabritius@ipa.fraunhofer.de
christoph.martin@ipa.fraunhofer.de

Andreas Pott
Fraunhofer Institute for Manufacturing Engineering and Automation (IPA)
Institute for Control Engineering of Machine Tools (ISW)
University of Stuttgart
Stuttgart, 70569
Germany
andreas.pott@isw.uni-stuttgart.de

ABSTRACT

Using fully-constrained cable robots as manipulators for 3D-printing, there is the risk of collisions between the cables and the printing part.
This paper presents a method to calculate the shape of the workspace volume within which a part can be printed without such collisions. The presented method is based on the fact that the printing part is produced in a sequence of horizontal layers. The areas occupied by the cables in the layers are scaled similar mappings of the cross-sections of the printing part. There is no collision if the 2D-shapes occupied by the cables in the printing layer do not overlap with the cross-sections of the printing part in the same layer. A procedure to find the largest printable 2D-shapes within the class of parallelograms for each layer is developed. The maximum printable 3D-volume is then given by stacking the 2D-shapes of each layer. Figures show the results of the method applied on the cable robot IPAnema 3. Finally, a guideline for the design of fully-constrained cable robots to maximize their printable volume is given.

INTRODUCTION

For the production of small-scale parts, additive manufacturing is an already well-established production technology. Using this technology for the production of large-scale concrete parts as depicted in Fig. 1 would be of great profit for the construction sector. It enables on-site production and new

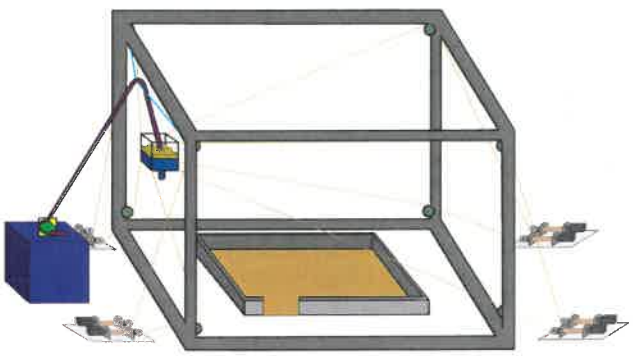

FIGURE 1: CONCEPT FOR LARGE-SCALE ADDITIVE MANUFACTURING [1]

*Address all correspondence to this author.

shapes without the need of formworks, which are necessary in applying the conventional method to keep the concrete in shape during the hardening process. Furthermore, it could reduce costs and production time compared to the conventional production method [2].
Large-scale additive manufacturing for the construction sector requires easily transportable robot kinematics with a large workspace, high accuracy and has to be able to carry high payloads. A robot class fulfilling these requirements are cable-driven parallel robots which are the subject of this paper.
Cable-driven parallel robots belong to the family of parallel robots. Their legs consist of cables which connect a rigid frame to a mobile platform. Through changing the length of these cables by winches, the platform can be moved.
Using cable robots, collisions can significantly restrict the workspace. Thus, they have to be considered in the design phase of a cable robot and during its operation. The occurring collision types can be categorized in cable-cable, cable-platform, platform-environment and cable-environment collisions [3].
Several works, studying the determination of cable-cable collisions can be found [3–6]. In [3], an algorithm is presented which can detect the occurrence of cable-cable collisions when moving the platform between two poses. For the determination of the collision-free workspace, Merlet and Perreault et al. [4, 5] propose a method to determine the cable-cable interference regions for constant orientation through a geometrical approach.
Collisions between cables and platform have been studied for example in [3, 4]. The method proposed in [3] simplifies the platform geometry by only considering the convex hull of the platform. In [4], the platform shape is approximated by a polyhedron. Thus, interferences between the convex hull and the cables or the polyhedron and the cables can be checked. With another approach developed by Pott [7], the maximum deflection angles of the cables at the distal anchor points of the platform can be calculated and used for cable-platform collision analysis.
For the cable-environment and platform-environment collision problem, only a few works can be found. Martin et al. [8] present a method to determine the interference regions where a collision between the cables and an object in shape of a cylinder occurs. The interference volume is determined by tangents of the cables on the boundary of the cylinder which is described in a closed-form. In [9], for the detection of collisions between the cable robot and the environment, it is also proposed to use simple geometric shapes like cylinders or spheres to model the environment. If more complex shapes have to be checked for collisions, they are described by polygonal meshes. The collision is analysed by calculating the distances between the edges of the polygon and the cables. Bosscher et al. [2] address the cable-environment collision problem of a fully-constrained cable robot for contour crafting by moving the proximal anchor points of the lower cables upwards during the printing process by four additional actuators.

To the best of the authors' knowledge, no method can be found in the literature to determine the collision-free workspace of fully-constrained cable robots in terms of cable-object collision for layer-based production processes where the object grows layer by layer. The proposed approach in this paper regards the layer-based production process of 3D-printing, but the presented method is not limited to 3D-printing. It is applicable for all layer-based production processes, for example automated brick laying with cable robots as proposed in [10] and [11].

The method presented in this paper first calculates the largest printable 2D-shapes for each layer. Parallelograms are used for the mathematical description of the horizontal cross-sections of the printing workspace. The method exploits the fact that the 2D-shapes of the point set defined by the points where the cables penetrate the printing layer are similar to the cross-section of the printing part in the printing layer. In a second step, it is checked whether the calculated largest printable 2D-shapes in each layer are printable without any interdependence on other 2D-shapes in other layers. The resulting printable volume which consists of the stacked 2D-shapes of each layer resembles an approximation of the collision-free printing workspace.
The so calculated collision-free printing workspace only addresses the geometric constraints on the workspace imposed by collisions. Clearly, within a design process of a cable robot, other criteria such as wrench-feasibility, velocity feasibility, and reachability have to be taken into account.

Kinematic model of a cable robot for 3D-printing

Based on Fig. 2, the geometry and kinematic model of a cable robot for the application of 3D-printing is explained in the following. Consider a cable-driven parallel robot with m cables. Each cable i with the index $i \in \{1,...,m\}$ is attached to a winch at its proximal anchor point whose position is defined by the vector $\mathbf{a}_i \in \mathbb{R}^3$ in the fixed frame coordinate system $\mathscr{K}_0$. The coordinate system $\mathscr{K}_0$ is spanned by the Cartesian unit vectors $\mathbf{e}_1, \mathbf{e}_2, \mathbf{e}_3 \in \mathbb{R}^3$. The other end of the i-th cable is connected to the platform at its distal anchor point whose coordinates are denoted as $\mathbf{b}_i \in \mathbb{R}^3$ in the platform coordinate system $\mathscr{K}_\mathrm{P}$. Within the approach presented in this paper, no rotations of the platform are considered for the application of 3D-printing. Therefore, the transformation between the coordinate systems $\mathscr{K}_0$ and $\mathscr{K}_\mathrm{P}$ is a simple translation given by the vector of the platform position $\mathbf{r} \in \mathbb{R}^3$. Equation (1) expresses the cable vector $\mathbf{l}_i$ from the distal to the proximal anchor point of each cable i in $\mathscr{K}_0$.

$$\mathbf{l}_i = \mathbf{a}_i - (\mathbf{r} + \mathbf{b}_i) \tag{1}$$

The printing nozzle which extrudes the printing material is connected to the mobile platform and is modeled with the vector $\mathbf{p}$.

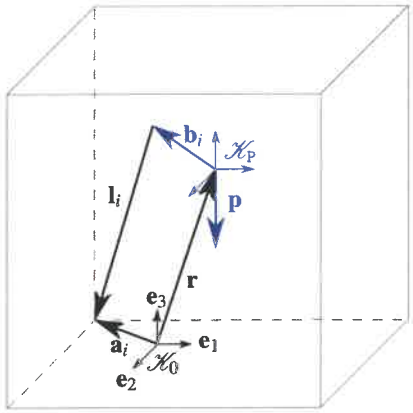

FIGURE 2: GEOMETRY MODEL OF A CABLE ROBOT FOR 3D-PRINTING

This vector denotes the position of the extrusion point of the printing material in the platform coordinate system $\mathscr{K}_P$.

Assumptions and Constraints

The approach presented in this paper is based on the following assumptions and notations:

- The standard cable model is assumed, i.e. all cables $i = 1,...,m$ of the robot are considered to be straight line segments between their distal and proximal anchor points $\mathbf{b}_i$ and $\mathbf{a}_i$. Therefore, each of them can be described by its cable vector $\mathbf{l}_i$.
- The distal anchor points $\mathbf{b}_i$ of all cables $i = 1,...,m$ are above the extrusion point of the printing nozzle: $h_i^P = \langle \mathbf{b}_i - \mathbf{p}, \mathbf{e}_3 \rangle \geq 0$. Herein $\langle \cdot, \cdot \rangle$ denotes the scalar product of two vectors.
- The 3D-printing process is structured in horizontal layers, which means the printing part is built up through consecutive layers of printing material starting from the bottom. Without loss of generality, it is assumed that the normal of the printing layers is aligned with the $\mathbf{e}_3$-axis of the fixed frame coordinate system $\mathscr{K}_0$.
- There is no restriction on the order in which the cross-sections of the printing part in each horizontal layer can be printed.
- The reduction of a vector $\mathbf{x} \in \mathbb{R}^3$ to its horizontal components is denoted as $\mathbf{x}_{(\mathbf{e}_1,\mathbf{e}_2)} = (\langle \mathbf{x}, \mathbf{e}_1 \rangle, \langle \mathbf{x}, \mathbf{e}_2 \rangle)^T \in \mathbb{R}^2$. The horizontal unit vectors are denoted by $\tilde{\mathbf{e}}_1 := \mathbf{e}_{1(\mathbf{e}_1,\mathbf{e}_2)} \in \mathbb{R}^2$ and $\tilde{\mathbf{e}}_2 := \mathbf{e}_{2(\mathbf{e}_1,\mathbf{e}_2)} \in \mathbb{R}^2$.
- The cross-sections of the printing workspace i.e. the largest printable 2D-shapes in each layer are described by parallelograms.
- The parallelograms are printed around the center points $\mathbf{c}$, whose horizontal components $\mathbf{c}_{(\mathbf{e}_1,\mathbf{e}_2)}$ are the same in all layers. The height of each layer is given by $h = \langle \mathbf{c}, \mathbf{e}_3 \rangle$.

Printing in a horizontal layer

From the center of the platform at the position $\mathbf{r}$, the printing nozzle extends downwards to extrude the printing material at the point $\mathbf{r} + \mathbf{p}$ with respect to $\mathscr{K}_0$.

The first observation considering collisions between the printing shapes and cables is that not all m cables of the robot are necessarily relevant regarding such collisions during the printing process in a horizontal layer. Only cables that cross the printing layer are relevant. For each cable $i = 1,...,m$, the relative height of the printing layer is defined as $h_i = h - \langle \mathbf{a}_i, \mathbf{e}_3 \rangle$. Due to the assumption $h_i^P = \langle \mathbf{b}_i - \mathbf{p}, \mathbf{e}_3 \rangle \geq 0$, a cable i is *relevant* if and only if its proximal anchor point $\mathbf{a}_i$ lies below the printing layer i.e. if its relative height is non-negative $h_i \geq 0$.

When the printing nozzle is extruding printing material at $\mathbf{c}$, each of the *relevant* cables i crosses the printing layer h_i at a point $\mathbf{s}_i^{\mathbf{c},h_i}$, which can be thought as an affine mapping of $\mathbf{c}$ cast by the cable i. The location of this image point $\mathbf{s}_i^{\mathbf{c},h_i}$ can be geometrically

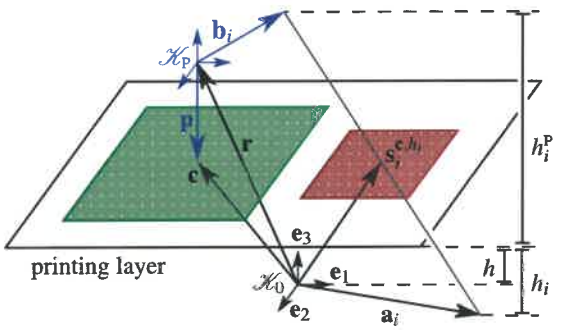

FIGURE 3: GEOMETRIC CONSTRUCTION OF THE IMAGE POINT $\mathbf{s}_i^{\mathbf{c},h_i}$

constructed as illustrated in Fig. 3 and described by the following formula

$$\mathbf{s}_i^{\mathbf{c},h_i} = \mathbf{a}_i + f_i^{h_i} \left((\mathbf{c} - \mathbf{p} + \mathbf{b}_i) - \mathbf{a}_i \right) . \tag{2}$$

The scalar factor $f_i^{h_i}$ describes the portion of the cable which is below the printing plane

$$f_i^{h_i} = \frac{h_i}{h_i^P + h_i} \in [0,1] . \tag{3}$$

While the printing nozzle is printing a shape in the horizontal layer, its similarly moving image point $\mathbf{s}_i^{\mathbf{c},h_i}$ traces the affine map-

ping in the same layer. This image of the printed shape is scaled by the factor $f_i^{h_i}$ from Eqn. (3). Based on these mappings, a simple criterion can be formulated to determine whether a shape belongs to the printing workspace so that there are no cable collisions with the shape during the printing process:

A 2D-shape can be printed in an arbitrary order if and only if it does not overlap with any of its affine mappings.

This motivates the following definitions:

- $\mathscr{P}_i^{h_i}$ is the set of 2D-shapes in the printing layer of height h which do not overlap with their image cast by the *relevant* cable i. The shapes in this set are said to be printable with respect to cable i.
- $\mathscr{P}_{\text{all}}^{h} = \bigcap_i \mathscr{P}_i^{h_i}$ is the set of 2D-shapes in the printing layer of height h which do not overlap with any images cast by the *relevant* cables. The shapes in this set are said to be printable with respect to all relevant cables.

Approximation of the printing workspace

To systematically address the question whether 2D-shapes belong to the printing workspace in a horizontal layer, i.e. are contained in $\mathscr{P}_{\text{all}}^{h}$, the class of parallelograms which is characterized by few parameters is considered. This allows the explicit calculation of the optimal size parameters which correspond to the largest printable parallelograms.

$\mathscr{P}_{\mathbf{d}_1,\mathbf{d}_2}$ denotes the class of parallelograms in $\mathbb{R}^2$ around the center $\mathbf{c}_{(\mathbf{e}_1,\mathbf{e}_2)} \in \mathbb{R}^2$ with the linear independent principal axis $\mathbf{d}_1, \mathbf{d}_2 \in \mathbb{R}^2$ and two free parameters (a_1, a_2) with $a_1, a_2 > 0$ that specify the size of its elements.

The parallelogram $p(a_1, a_2) \in \mathscr{P}_{\mathbf{d}_1,\mathbf{d}_2}$ with sizes $a_1, a_2 > 0$ contains all points in the set

$$\left\{ \mathbf{c}_{(\mathbf{e}_1,\mathbf{e}_2)} + x_1\mathbf{d}_1 + x_2\mathbf{d}_2 \mid x_1 \in [-a_1, a_1],\ x_2 \in [-a_2, a_2] \right\} . \quad (4)$$

Since the class $\mathscr{P}_{\mathbf{d}_1,\mathbf{d}_2}$ has two independent size parameters, there usually exist two printable parallelograms of infinite size in $\mathscr{P}_{\mathbf{d}_1,\mathbf{d}_2} \cap \mathscr{P}_i^{h_i}$. To deal with this multiplicity, the concept of *characteristic* parallelograms is introduced.

The space between the center $\mathbf{c}$ and its image point $\mathbf{s}_i^{\mathbf{c},h_i}$ has to be split up between the printable parallelogram around $\mathbf{c}$ and its affine mapping which is centered at $\mathbf{s}_i^{\mathbf{c},h_i}$. The factor $f_i^{h_i}$ from Eqn. (3) implies the partition of the spanning vector $\left(\mathbf{s}_i^{\mathbf{c},h_i} - \mathbf{c}\right)_{(\mathbf{e}_1,\mathbf{e}_2)}$ according to the ratios

$$\frac{1}{1+f_i^{h_i}} \quad \text{and} \quad \frac{f_i^{h_i}}{1+f_i^{h_i}} . \quad (5)$$

The printable *characteristic* parallelogram resulting from this partition is spanned by

$$\mathbf{v}_i^{h_i} = \frac{\left(\mathbf{s}_i^{\mathbf{c},h_i} - \mathbf{c}\right)_{(\mathbf{e}_1,\mathbf{e}_2)}}{1+f_i^{h_i}} . \quad (6)$$

The signed versions $a_1^{\pm}, a_2^{\pm}$ of the parameters $a_1 = |a_1^{\pm}|$, $a_2 = |a_2^{\pm}|$ of the parallelogram $p\left(|a_1^{\pm}|, |a_2^{\pm}|\right)$ satisfy the relationship

$$\begin{bmatrix} a_1^{\pm} \\ a_2^{\pm} \end{bmatrix} = \mathbf{Q}^{-1}\mathbf{v}_i^{h_i} \qquad \text{where } \mathbf{Q} = \begin{bmatrix} \mathbf{d}_1\ \mathbf{d}_2 \end{bmatrix} \in \mathbb{R}^{2\times 2} . \quad (7)$$

Figure 4 illustrates the geometric construction of this parallelogram. The green and red areas represent one quarter of the *characteristic* parallelogram $p(a_1, a_2)$ and its image $p\left(f_i^{h_i}a_1, f_i^{h_i}a_2\right)$. The areas marked with checkerboard patterns show that an extension of the *characteristic* parallelogram in its first parameter a_1 does not cause an overlap with the accordingly extended image.

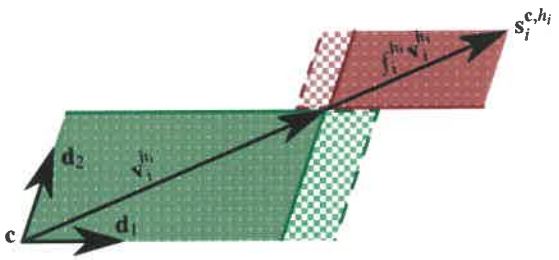

FIGURE 4: GEOMETRIC CONSTRUCTION OF THE *CHARACTERISTIC* PARALLELOGRAM IN $\mathscr{P}_i^{h_i}$.

This printable extension could also be made in the second parameter a_2 instead. From this observation, it becomes apparent that the *characteristic* parallelogram $p(a_1, a_2)$ is the largest parallelogram, so that both sides can be individually extended to the printable parallelograms $p(a_1, +\infty)$ and $p(+\infty, a_2)$. These are the largest printable parallelograms in terms of area in $\mathscr{P}_{\mathbf{d}_1,\mathbf{d}_2} \cap \mathscr{P}_i^{h_i}$. If $\mathbf{v}_i^{h_i}$ is parallel to one of the principal axis $\mathbf{d}_1$ or $\mathbf{d}_2$, its corresponding size parameter $a_1^{\pm}$ or $a_2^{\pm}$ has the value 0. For such a configuration, only one of the mentioned parallelograms will be a valid printable parallelogram in $\mathscr{P}_{\mathbf{d}_1,\mathbf{d}_2}$. Depending on the geometry of the robot, there may also be multiple largest parallelograms in $\mathscr{P}_{\mathbf{d}_1,\mathbf{d}_2} \cap \mathscr{P}_{\text{all}}^{h}$ in terms of area.

Before this multiplicity can be dealt with, Algorithm 1 creates a list $\mathscr{L}_1$ containing the *characteristic* parallelogram sizes of all

relevant cables. The input arguments of Algorithm 1 are the fixed parameters of $\mathscr{P}_{\mathbf{d}_1,\mathbf{d}_2}$ and the center $\mathbf{c}$. In Line 1, the list $\mathscr{L}_1$ is initialized. While iterating over all cables, a check is performed in Line 2 to skip over the *irrelevant* ones. The scaling factor $f_i^{h_i}$ and the image point $\mathbf{s}_i^{\mathbf{c},h_i}$ of the center $\mathbf{c}$ are calculated in Lines 3 and 4 followed by $\mathbf{v}_i^{h_i}$ and the signed parameters $a_1^{\pm}, a_2^{\pm}$ in Lines 5 and 6. In Line 7, the absolute values of these parameters i.e. the size parameters of the *characteristic* parallelogram in $\mathscr{P}_{\mathbf{d}_1,\mathbf{d}_2} \cap \mathscr{P}_i^{h_i}$ are added to the list $\mathscr{L}_1$.

Algorithm 1: Calculate list of *characteristic* parallelogram sizes $\mathscr{L}_1$

Input: center $\mathbf{c} \in \mathbb{R}^3$, principal axis $\mathbf{d}_1, \mathbf{d}_2 \in \mathbb{R}^2$, cable robot geometry $\{\mathbf{a}_i, \mathbf{b}_i, \mathbf{p}\}$
Output: *characteristic* parallelogram sizes $\mathscr{L}_1$

$\mathbf{Q} = \begin{bmatrix}\mathbf{d}_1 & \mathbf{d}_2\end{bmatrix}$
1 $\mathscr{L}_1 := \{\}$
for *cable* $i = 1, ..., m$ **do**
  $h_i := \langle \mathbf{c} - \mathbf{a}_i, \mathbf{e}_3 \rangle$
  $h_i^{\mathrm{P}} := \langle \mathbf{b}_i - \mathbf{p}, \mathbf{e}_3 \rangle$
2 **if** $h_i < 0$ **then continue**
3 $f_i^{h_i} := \frac{h_i}{h_i^{\mathrm{P}} + h_i}$
4 $\mathbf{s}_i^{\mathbf{c},h_i} = \mathbf{a}_i + f_i^{h_i}\left((\mathbf{c} - \mathbf{p} + \mathbf{b}_i) - \mathbf{a}_i\right)$
5 $\mathbf{v}_i^{h_i} := \frac{\left(\mathbf{s}_i^{\mathbf{c},h_i} - \mathbf{c}\right)_{(\mathbf{e}_1,\mathbf{e}_2)}}{1 + f_i^{h_i}}$
6 $\begin{bmatrix}a_1^{\pm} \\ a_2^{\pm}\end{bmatrix} := \mathbf{Q}^{-1}\mathbf{v}_i^{h_i}$
7 $\mathscr{L}_1 = \left\{\mathscr{L}_1, \left(\left|a_1^{\pm}\right|, \left|a_2^{\pm}\right|\right)\right\}$
end
return $\mathscr{L}_1$

Algorithm 2 processes this list to extract all parameter combinations that resemble printable parallelograms in $\mathscr{P}_{\mathbf{d}_1,\mathbf{d}_2} \cup \mathscr{P}_{\mathrm{all}}^{h}$. Firstly, the entry $(+\infty, +\infty)$ is added to the list $\mathscr{L}_1$ in Line 1. This is done to account for the possibility that one parameter of a printable parallelogram could be infinite. Then, an iteration over all combinations of parameter tuples (a_1, a_2) (set in the Lines 2 and 3) in $\mathscr{L}_1$ is started. In Line 4, each parameter combination is compared to all printable parameter pairs in $\mathscr{L}_1$. If both a_1 and a_2 are larger than the corresponding sizes of any entry from the list, the parallelogram $p(a_1, a_2) \notin \mathscr{P}_{\mathrm{all}}^{h}$ is not printable. Parameter tuples that pass this test are in $\mathscr{P}_{\mathrm{all}}^{h}$ and are added to the list

Algorithm 2: Calculate list of printable parallelogram sizes $\mathscr{L}_2$

Input: *characteristic* parallelogram sizes $\mathscr{L}_1$
Output: sorted list of printable parallelogram sizes $\mathscr{L}_2$ in $\mathscr{P}_{\mathbf{d}_1,\mathbf{d}_2} \cap \mathscr{P}_{\mathrm{all}}^{h}$

$\mathscr{L}_2 := \{\}$
1 $\mathscr{L}_1 = \{\mathscr{L}_1, (+\infty, +\infty)\}$
for $i = 1, ..., \mathscr{L}_1.size()$ **do**
  for $j = 1, ..., \mathscr{L}_1.size()$ **do**
2 $a_1 := \mathscr{L}_1(i, 1)$
3 $a_2 := \mathscr{L}_1(j, 2)$
  printable = **true**
  for $k = 1, ..., \mathscr{L}_1.size() - 1$ **do**
4 **if** $(\mathscr{L}_1(k, 1) < a_1)$ **and** $(\mathscr{L}_1(k, 2) < a_2)$ **then** *printable* = **false**
  end
5 **if** *printable* = **true then**
6 $\mathscr{L}_2 = \{\mathscr{L}_2, (a_1, a_2)\}$
  end
end
7 sort $(\mathscr{L}_2)$
return $\mathscr{L}_2$

$\mathscr{L}_2$ in Line 6. The rows of this list are then sorted in Line 7 into descending order with respect to the area of the parallelograms. Figure 5 shows the four largest printable parallelograms calculated by Algorithm 1 and 2. The calculation is performed with the parameters in [m]:

$$\begin{aligned}\mathbf{p} &= \begin{bmatrix}0.0 & 0.0 & -0.3\end{bmatrix}^{\mathsf{T}}, \ \mathbf{c} = \begin{bmatrix}0.0 & 0.0 & -0.3\end{bmatrix}^{\mathsf{T}}, \\ \mathbf{d}_1 &= \begin{bmatrix}0.6 & 1.0\end{bmatrix}^{\mathsf{T}}, \ \mathbf{d}_2 = \begin{bmatrix}0.6 & -1.0\end{bmatrix}^{\mathsf{T}},\end{aligned} \tag{8}$$

for the cable robot IPAnema 3. Table 1 lists the vectors of the IPAnema 3 proximal anchor points with respect to the coordinate system $\mathscr{K}_0$ and the distal anchor points with respect to $\mathscr{K}_{\mathrm{P}}$. Note that the parallelograms in Figs. 5a and 5c appear at the top of the list $\mathscr{L}_2$ because one of their size parameters was set to a very large constant in the implementation of Line 1 from Algorithm 2.

Interdependence of horizontal printing layers

In the previous sections, only collision-free printing within a single layer (of height) h has been discussed. To print 3D-objects

cable i	$\mathbf{a}_i$ [m]	$\mathbf{b}_i$ [m]
1	$[\ 3.757,\ 5.376,\ 1.882]^\mathsf{T}$	$[\ 0.248,\ 0.110, -0.167]^\mathsf{T}$
2	$[\ 4.043, -5.376,\ 1.863]^\mathsf{T}$	$[\ 0.248, -0.110, -0.167]^\mathsf{T}$
3	$[-4.043, -5.557,\ 1.878]^\mathsf{T}$	$[-0.248, -0.110, -0.167]^\mathsf{T}$
4	$[-4.340,\ 5.233,\ 1.873]^\mathsf{T}$	$[-0.248,\ 0.110, -0.167]^\mathsf{T}$
5	$[\ 3.185,\ 5.796, -1.870]^\mathsf{T}$	$[\ 0.110,\ 0.248,\ 0.167]^\mathsf{T}$
6	$[\ 4.073, -5.589, -1.903]^\mathsf{T}$	$[\ 0.110, -0.248,\ 0.167]^\mathsf{T}$
7	$[-3.811, -5.738, -1.888]^\mathsf{T}$	$[-0.110, -0.248,\ 0.167]^\mathsf{T}$
8	$[-3.993,\ 5.441, -1.882]^\mathsf{T}$	$[-0.110,\ 0.248,\ 0.167]^\mathsf{T}$

TABLE 1: Geometrical parameters of the cable robot IPAnema 3

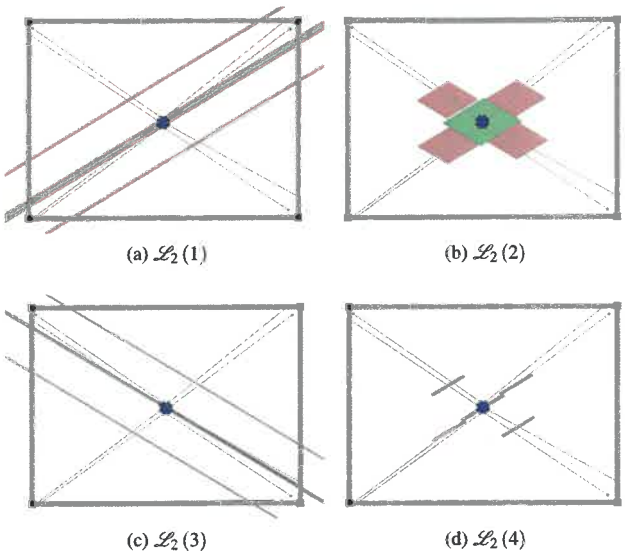

(a) $\mathscr{L}_2(1)$ (b) $\mathscr{L}_2(2)$

(c) $\mathscr{L}_2(3)$ (d) $\mathscr{L}_2(4)$

FIGURE 5: LARGEST PARALLELOGRAMS CALCULATED BY ALGORITHM 2

made up of many vertically stacked layers in a height interval $[h_{\min}, h_{\max}]$, cable collisions with the cross-sections in all the other layers have to be avoided. When printing in the layer $h+\Delta h$ with $\Delta h > 0$, the cables should neither collide with the printing shape inside this layer, nor with any previously printed shape in a lower layer h.

To simplify the task of finding the largest printable shapes in all layers $h \in [h_{\min}, h_{\max}]$ which satisfy these criteria, a condition is sought under which the interdependence between these layers can be neglected. The idea is that such a condition would guarantee that for each cross-section, the constraints on its largest printable shape due to the affine mappings cast from the cables within this layer are stricter than those due to the following cross-sections in higher layers.

Let $\mathscr{P}_{i,\Delta h}^{h_i}$ be the set of 2D-shapes in the printing layer of height h_i which do not overlap with the image of the printed shape in the layer $h_i + \Delta h$ cast by the *relevant* cable i. The shapes in this set are said to be printable with respect to the layer $h_i + \Delta h$ and cable i.

With this definition, the condition which allows to neglect the interdependence of the shapes in the layers of the relative height interval $[h_{i,\min}, h_{i,\max}] = [h_{\min} - \langle \mathbf{a}_i, \mathbf{e}_3 \rangle, h_{\max} - \langle \mathbf{a}_i, \mathbf{e}_3 \rangle]$, can be stated as

$$\begin{aligned} &\mathscr{P}_i^{h_i} \subseteq \mathscr{P}_{i,\Delta h}^{h_i} \\ &\forall h_i \in [h_{i,\min}, h_{i,\max}],\ \Delta h \in (0, h_{i,\max} - h_i] \end{aligned} \tag{9}$$

Before this condition can be adapted for the shape class of parallelograms $\mathscr{P}_{\mathbf{d}_1,\mathbf{d}_2}$, some general observations and notations need to be introduced. Note that the spanning vector $\mathbf{v}_i^{h_i}$ from Eqn. (6) of the *characteristic* parallelogram in $\mathscr{P}_i^{h_i}$ can also be constructed as the distance vector between $\mathbf{c}$ and $\mathbf{s}_i^{\mathbf{c},h_i}$ minus the spanning vector of the corresponding affine mapping. This construction can also be used to define the *characteristic* parallelogram in $\mathscr{P}_{i,\Delta h}^{h_i}$. The affine mapping cast by cable i in layer h_i while printing in layer $h_i + \Delta h$ can also be thought of as being the result of printing in the layer h_i with an extended printing nozzle $\mathbf{p}_{\Delta h} = \mathbf{p} - \Delta h \mathbf{e}_3$. The resulting image point $\mathbf{s}_{i,\Delta h}^{\mathbf{c},h_i}$ in the layer h_i is calculated by adapting Eqn. (2) to the extended printing nozzle

$$\mathbf{s}_{i,\Delta h}^{\mathbf{c},h_i} = \mathbf{a}_i + f_{i,\Delta h}^{h_i} \left((\mathbf{c} - \mathbf{p}_{\Delta h} + \mathbf{b}_i) - \mathbf{a}_i \right), \tag{10}$$

with the scaling factor

$$f_{i,\Delta h}^{h_i} = \frac{h_i}{h_i^\mathrm{P} + h_i + \Delta h}. \tag{11}$$

The size of the corresponding affine mapping depends on the image of the *characteristic* parallelogram in the higher layer $h_i + \Delta h$. Its size is given by the spanning vector $f_i^{h_i+\Delta h} \mathbf{v}_i^{h_i+\Delta h}$. When the area of this image is projected onto the layer h_i, it shrinks according to the factor $\frac{h_i}{h_i+\Delta h}$. This observation can be combined with the formula from Eqn. (10) to obtain the spanning vector $\mathbf{v}_{i,\Delta h}^{h_i}$.

$$\begin{aligned} \mathbf{v}_{i,\Delta h}^{h_i} &= \left(\mathbf{s}_{i,\Delta h}^{\mathbf{c},h_i} - \mathbf{c} \right)_{(\mathbf{e}_1,\mathbf{e}_2)} - \frac{h_i}{h_i + \Delta h} f_i^{h_i+\Delta h} \mathbf{v}_i^{h_i+\Delta h} \\ &= \frac{(\mathbf{b}_i - \mathbf{p})_{(\mathbf{e}_1,\mathbf{e}_2)} h_i + (\mathbf{a}_i - \mathbf{c})_{(\mathbf{e}_1,\mathbf{e}_2)} (h_i^\mathrm{P} + 2\Delta h)}{h_i^\mathrm{P} + 2h_i + 2\Delta h} \end{aligned} \tag{12}$$

This vector describes the *characteristic* printable parallelogram in layer h_i with respect to the affine mapping cast by cable i due to the *characteristic* parallelogram in the higher layer $h_i + \Delta h$.
To adapt the condition in Eqn. (9) for the case of parallelograms in $\mathscr{P}_{\mathbf{d}_1,\mathbf{d}_2}$, the derivative of $\mathbf{v}_{i,\Delta h}^{h_i}$ with respect to Δh is calculated by

$$\frac{\mathrm{d}}{\mathrm{d}\Delta h}\mathbf{v}_{i,\Delta h}^{h_i} = \frac{(\mathbf{b}_i - \mathbf{p})_{(\mathbf{e}_1,\mathbf{e}_2)}(-2h_i) + (\mathbf{a}_i - \mathbf{c})_{(\mathbf{e}_1,\mathbf{e}_2)}(4h_i)}{\left(h_i^{\mathrm{P}} + 2h_i + 2\Delta h\right)^2}. \quad (13)$$

Note that the direction of this derivative does not depend on Δh. The idea is that if both parameters (a_1, a_2) of the *characteristic* parallelograms in $\mathscr{P}_{\mathbf{d}_1,\mathbf{d}_2} \cap \mathscr{P}_{i,\Delta h}^{h_i}$ which are defined by $\mathbf{v}_{i,\Delta h}^{h_i}$ grow for increasing Δh, the smallest *characteristic* parallelogram in this group is the one in $\mathscr{P}_{\mathbf{d}_1,\mathbf{d}_2} \cap \mathscr{P}_i^{h_i}$ which is spanned by $\mathbf{v}_i^{h_i} = \mathbf{v}_{i,0}^{h_i}$. Figure 6 illustrates a setting where this condition is satisfied.

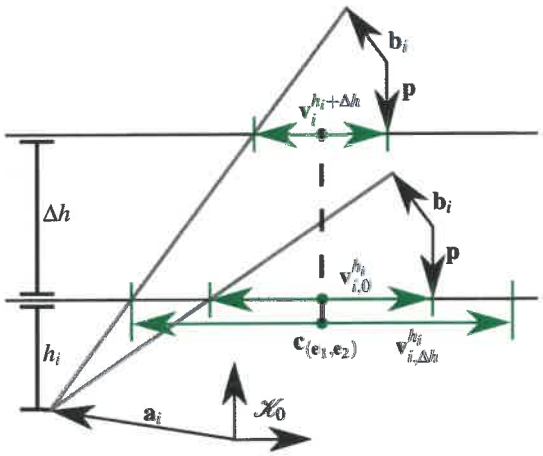

FIGURE 6: VISUALIZATION OF THE INTERDEPENDENCE CRITERION

The other *characteristic* parallelograms which are defined through affine mappings cast from the cables in higher layers $h_i + \Delta h$ can then be neglected since they are larger.
Based on the relationship between the signed parameters $a_k = \{a_1^{\pm}, a_2^{\pm}\}$ of the *characteristic* parallelogram and its spanning vector from Eqn. (7), the condition from Eqn. (9) can be expressed as

$$\begin{aligned} &\frac{\mathrm{d}}{\mathrm{d}\Delta h}a_k^2 \geq 0 \\ \iff &2a_k\frac{\mathrm{d}}{\mathrm{d}\Delta h}a_k \geq 0 \\ \iff &2\left\langle \mathbf{Q}^{-1}\mathbf{v}_{i,\Delta h}^{h_i}, \widetilde{\mathbf{e}}_k\right\rangle \left\langle \mathbf{Q}^{-1}\frac{\mathrm{d}}{\mathrm{d}\Delta h}\mathbf{v}_{i,\Delta h}^{h_i}, \widetilde{\mathbf{e}}_k\right\rangle \geq 0 \\ &k = \{1,2\}, \forall\, h_i \in [h_{i,\min}, h_{i,\max}],\ \Delta h \in (0, h_{i,\max} - h_i] \end{aligned} \quad (14)$$

Since only the signs of the expressions in this criterion matter, all positive factors can be omitted

$$\begin{aligned} &2\left\langle \mathbf{Q}^{-1}\mathbf{v}_{i,\Delta h}^{h_i}, \widetilde{\mathbf{e}}_k\right\rangle \left\langle \mathbf{Q}^{-1}\frac{\mathrm{d}}{\mathrm{d}\Delta h}\mathbf{v}_{i,\Delta h}^{h_i}, \widetilde{\mathbf{e}}_k\right\rangle \geq 0 \\ \iff &\left\langle \mathbf{Q}^{-1}\left((\mathbf{b}_i - \mathbf{p})_{(\mathbf{e}_1,\mathbf{e}_2)}h_i + (\mathbf{a}_i - \mathbf{c})_{(\mathbf{e}_1,\mathbf{e}_2)}h_i^{\mathrm{P}}\right), \widetilde{\mathbf{e}}_k\right\rangle \\ &\cdot\left\langle \mathbf{Q}^{-1}\left(-(\mathbf{b}_i - \mathbf{p})_{(\mathbf{e}_1,\mathbf{e}_2)} + 2(\mathbf{a}_i - \mathbf{c})_{(\mathbf{e}_1,\mathbf{e}_2)}\right), \widetilde{\mathbf{e}}_k\right\rangle \geq 0\,. \end{aligned} \quad (15)$$

With this simplification, it becomes apparent that it suffices to only check Eqn. (15) for $\widetilde{\mathbf{e}}_k = \{\widetilde{\mathbf{e}}_1, \widetilde{\mathbf{e}}_2\}$ and the boundaries of the height interval $h_i = \{h_{i,\min}, h_{i,\max}\}$.
As mentioned before, *characteristic* parallelograms have the property that one of their size parameters can be increased without loosing the printability of the parallelogram with respect to the associated *relevant* cable. If the *characteristic* parallelogram in $\mathscr{P}_i^{h_i}$ and the one in $\mathscr{P}_{i,\Delta h}^{h_i}$ are extended in different size parameters, this can render the resulting parallelogram in layer $h_i + \Delta h$ unprintable with respect to a parallelogram in the layer h_i. Such a setting is illustrated in Fig. 7 where the extended parallelogram from $\mathbf{v}_i^{h_i}$ is shown in green and the affine mapping resulting from the extension of the parallelogram spanned by $\mathbf{v}_{i,\Delta h}^{h_i}$ is colored red. Since there is an overlap of the parallelogram and its image, the shown green parallelogram is not printable. Therefore it can be concluded that in general $\mathscr{P}_{\mathbf{d}_1,\mathbf{d}_2} \cap \mathscr{P}_i^{h_i}$ is not a subset of $\mathscr{P}_{\mathbf{d}_1,\mathbf{d}_2} \cap \mathscr{P}_{i,\Delta h}^{h_i}$ even if the criterion from Eqn. (15) holds.
The overlap from Fig. 7 can be avoided by extending both parallelograms in the same dimension. This is illustrated in Fig. 8.
Since the *characteristic* parallelogram in $\mathscr{P}_{i,\Delta h}^{h_i}$ is induced by the one in $\mathscr{P}_i^{h_i+\Delta h}$ from the higher layer $h_i + \Delta h$, overlaps as in Fig. 7 can be entirely avoided by extending all *characteristic* parallelograms in all layers $h_i \in [h_{i,\min}, h_{i,\max}]$ in the same size parameter.

To select the size parameter for each *relevant* cable i that is extended in all layers h_i, the following procedure is implemented.
Firstly, the list of printable parallelograms $\mathscr{L}_2$ is calculated by the Algorithms 1 and 2 for the lowest layer $h_{\min}$ in the printing height interval $[h_{\min}, h_{\max}]$.

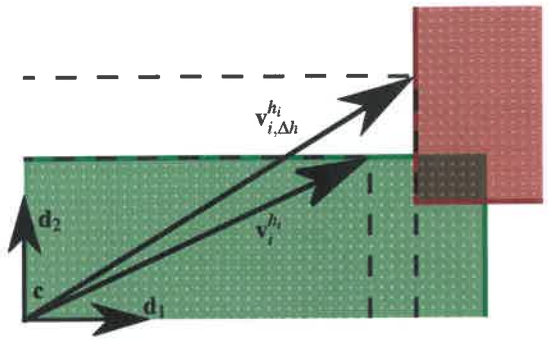

FIGURE 7: OVERLAP OF EXTENDED PARALLELOGRAM AND IMAGE BASED ON $\mathbf{v}_i^{h_i}$ AND $\mathbf{v}_{i,\Delta h}^{h_i}$

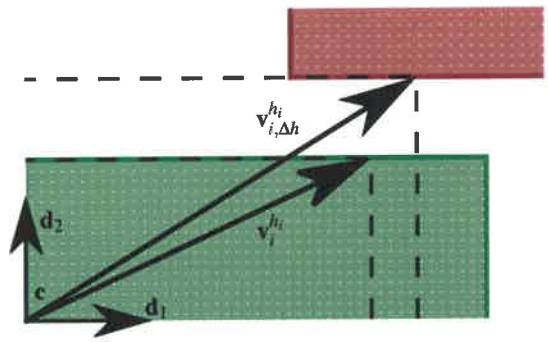

FIGURE 8: SETTING OF FIG. 7 WITHOUT OVERLAP

From this list, a suitable pair of parallelogram sizes is selected and for each *relevant* cable i, the information of which size parameter is not extended gets saved in a new list $\mathscr{L}_3$. The entries in this list $\mathscr{L}_3(i)$ either have the value 1 or 2 depending on which parameter is not allowed to be extended. To select a printable parallelogram in the higher layers $h_i + \Delta h$ with $\Delta h > 0$, Algorithm 1 and a modified version of Algorithm 2 are employed.
The list $\mathscr{L}_3$ is given as an input argument to Algorithm 2 and the following code is inserted before Line 5.

if $(\mathscr{L}_3(i) = 2$ **and** $a_2 > \mathscr{L}_1(i,2))$ **or**
$(\mathscr{L}_3(j) = 1$ **and** $a_1 > \mathscr{L}_1(j,1))$
then *printable* = **false**

This additional criterion ensures that for all *relevant* cables i, the *characteristic* parallelograms in each layer are extended in the same size parameter. From the sorted list $\mathscr{L}_2$ that is produced with this modification for each layer $h \in (h_{\min}, h_{\max}]$, the first i.e. the largest parallelograms are selected.
The approximation of the printing workspace formed by the parallelogram layers, calculated through this procedure, is visualized in Fig. 9. Hereby the same robot geometry and parameters are used as in Fig. 5. The calculation is performed for the height interval $[-1.75\,\mathrm{m}, 0.65\,\mathrm{m}]$.

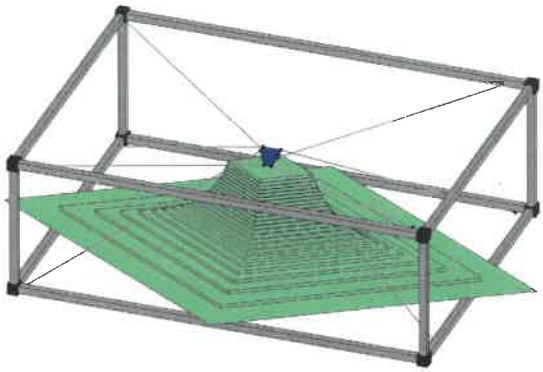

FIGURE 9: PRINTABLE VOLUME CONSISTING OF PARALLELOGRAM LAYERS

Design guidelines

The previous sections focused on the question whether 2D-shapes and 3D-objects can be printed by a given cable robot. In this section, the reverse problem is discussed.
Given the goal of printing large shapes and objects with a fully-constrained cable robot, the question is how to design the robot's geometry $\{\mathbf{a}_i, \mathbf{b}_i, \mathbf{p}\}_{i=1}^m$ in order to fulfill this objective.
This question can be addressed through the observation that the size of any printable convex shape in $\mathscr{P}_{\text{all}}^{h_i}$ around the center $\mathbf{c}$ in the layer h can be characterized by the vectors $\mathbf{v}_i^{h_i}$ of all relevant cables i from Eqn. (6). The expression for $\mathbf{v}_i^{h_i}$ can be reformulated in terms of the cable robot's geometry $\{\mathbf{a}_i, \mathbf{b}_i, \mathbf{p}\}$

$$\begin{aligned}\mathbf{v}_i^{h_i} &= \frac{\left(\mathbf{s}_i^{\mathbf{c},h_i} - \mathbf{c}\right)_{(\mathbf{e}_1,\mathbf{e}_2)}}{1 + f_i^{h_i}} \\ &= \frac{h_i}{h_i^{\mathrm{P}} + 2h_i}(\mathbf{b}_i - \mathbf{p})_{(\mathbf{e}_1,\mathbf{e}_2)} + \frac{h_i^{\mathrm{P}}}{h_i^{\mathrm{P}} + 2h_i}(\mathbf{a}_i - \mathbf{c})_{(\mathbf{e}_1,\mathbf{e}_2)}.\end{aligned} \tag{16}$$

From this formula, it becomes apparent that $\mathbf{v}_i^{h_i}$ is a linear combination of $(\mathbf{b}_i - \mathbf{p})_{(\mathbf{e}_1,\mathbf{e}_2)}$ and $(\mathbf{a}_i - \mathbf{c})_{(\mathbf{e}_1,\mathbf{e}_2)}$. Therefore the size of printable shapes which is directly related to the norm of this vector $\left\|\mathbf{v}_i^{h_i}\right\|$ can be maximized by obeying the following guidelines when designing a cable robot for the application of 3D-printing.

- The proximal anchor points $\mathbf{a}_i$ of all relevant cables i should be far away from each other so that the center of the printed shape $\mathbf{c}$ can be placed in their middle.
  As a result $\left\|(\mathbf{a}_i - \mathbf{c})_{(\mathbf{e}_1,\mathbf{e}_2)}\right\|$ should be large for all relevant cables i.
- For all relevant cables i, the vector $(\mathbf{b}_i - \mathbf{p})_{(\mathbf{e}_1,\mathbf{e}_2)}$ should point in the same direction as $(\mathbf{a}_i - \mathbf{c})_{(\mathbf{e}_1,\mathbf{e}_2)}$ and its norm $\left\|(\mathbf{b}_i - \mathbf{p})_{(\mathbf{e}_1,\mathbf{e}_2)}\right\|$ should be large.
- Since for most cable robots the robot frame is much larger than its platform $\left\|(\mathbf{a}_i - \mathbf{c})_{(\mathbf{e}_1,\mathbf{e}_2)}\right\| \gg \left\|(\mathbf{b}_i - \mathbf{p})_{(\mathbf{e}_1,\mathbf{e}_2)}\right\|$, the extrusion point of the printing nozzle should be far below the platform $h_i^{\mathrm{P}} \gg 0$.

Conclusion

In this paper, a method is presented to calculate the workspace within which a part can by generated by a 3D-printing process with a fully-constrained cable robot without collisions between the cables and the printing part. The method is based on an analysis of the largest printable 2D-shapes in each layer. For the description of the 2D-shapes, parallelograms are used. After a check of the interdependency between the horizontal layers, the largest printing workspace volume is described by stacking the printable 2D-shapes of each layer. Implementations of the methods and visualizations of the resulting largest printable shapes and volumes are provided. Finally, design guidelines for fully-constrained cable robots to maximize the printing workspace are derived.

The proposed method is not restricted to 3D-printing. It is suitable to calculate the largest feasible volume of a fully-constrained cable robot for any layer-based production process. Thus a useful tool is provided to evaluate the suitability of fully-constrained cable robots used as a manipulator for layer-based additive manufacturing.

Acknowledgements

The results presented in this paper are originated in the research project HINDCON (Hybrid INDustrial CONstruction) funded by the European Commission (Grant Agreement No 723611).

REFERENCES

[1] Fink, Marius. "Konzeptioneller Entwurf eines Seilroboters für das Large-Scale Manufacturing." Bachelor Thesis. Institute for Control Engineering of Machine Tools and Manufacturing, University of Stuttgart, Germany. 2017.

[2] Bosscher, Paul, Williams, Robert L., Bryson, L. Sebastian and Castro-Lacouture, Daniel. "Cable-suspended robotic contour crafting system." *Automation in Construction* Vol. 17 No. 1 (2007): pp. 45–55.

[3] Nguyen, Dinh Quan and Gouttefarde, Marc "On the Improvement of Cable Collision Detection Algorithms." *Cable-Driven Parallel Robots.* Springer International Publishing, Cham (2015): pp. 29–40.

[4] Merlet, Jean-Pierre. "Analysis of the influence of wires interference on the workspace of wire robots". *On Advances in Robot Kinematics.* Springer, Dordrecht (2004): pp. 211–218.

[5] Perreault, Simon, Cardou, Philippe, Gosselin, Clément M. and Otis, Martin J.-D. "Geometric determination of the interference-free constant-orientation workspace of parallel cable-driven mechanisms." *Journal of Mechanisms and Robotics* Vol. 2 No. 3 (2010): pp. 031016.

[6] Blanchet, Laurent and Merlet, Jean-Pierre. "Interference detection for cable-driven parallel robots (CDPRs)." *IEEE/ASME International Conference on Advanced Intelligent Mechatronics (AIM)* (2014): pp. 1413–1418.

[7] Pott, Andreas. "Determination of the cable span and cable deflection of cable-driven parallel robots." *Cable-Driven Parallel Robots.* Springer, Cham (2018): pp. 106–116.

[8] Martin, Antoine, Caro, Stéphane and Cardou, Philippe. "Geometric Determination of the Cable-Cylinder Interference Regions in the Workspace of a Cable-Driven Parallel Robot." *Cable-Driven Parallel Robots.* Springer, Cham (2018): pp. 117–127.

[9] Gagliardini, Lorenzo, Caro, Stéphane, Gouttefarde, Marc and Girin, Alexis "Discrete reconfiguration planning for cable-driven parallel robots". *Mechanism and Machine Theory* Vol. 100 (2016): pp. 313–337.

[10] Vukorep, Ilija. "Autonomous Big-Scale Additive Manufacturing Using Cable-Driven Robots." *ISARC. Proceedings of the International Symposium on Automation and Robotics in Construction* Vol. 34. Vilnius Gediminas Technical University, Department of Construction Economics & Property. 2017.

[11] Bruckmann, Tobias, Reichert, Christopher, Meik, Michael, Lemmen, Patrik, Spengler, Arnim, Mattern, Hannah and König, Markus. "Concept Studies of Automated Construction Using Cable-Driven Parallel Robots." *Cable-Driven Parallel Robots.* Springer, Cham (2018): pp. 364–375.